Reduced-Attitude Control of Fixed-Wing Unmanned Aerial Vehicles Using Geometric Methods on the Two-Sphere [*]

Erlend M. Coates [*] **Dirk Reinhardt** [*] **Thor I. Fossen** [*]

[*] *Center for Autonomous Marine Operations and Systems, Department of Engineering Cybernetics, Norwegian University of Science and Technology, 7491 Trondheim, Norway (e-mail: {erlend.m.l.coates,dirk.p.reinhardt,thor.fossen}@ntnu.no).*

Abstract: As an alternative to reduced-attitude control of fixed-wing unmanned aerial vehicles using roll and pitch angles, we propose to use a global representation that evolves on the two-sphere. The representation of reduced attitude is invariant to rotations about the inertial gravity axis, which makes it well suited for banked turn maneuvers. With the relative airspeed viewed as an exogenous input, a nonlinear controller for almost semiglobal exponential tracking of reduced attitude is presented. For the regulation case, asymptotic convergence is almost global, and the relationship to a classical approach using Euler angles is established. In addition to being singularity-free, a benefit of the presented approach is that the proportional action is pointed along the shortest direction on the sphere. The performance of the controller is demonstrated in numerical simulations.

Keywords: Aircraft control, Attitude control, Nonlinear control systems, Autonomous vehicles

1. INTRODUCTION

The attitude control system provides the main stabilization function in autopilots for fixed-wing unmanned aerial vehicles (UAVs). It enables a UAV to follow commands originating from outer-loop guidance schemes, thus allowing fully automatic flight. Guidance controllers typically achieve path-following or waypoint-tracking capabilities by controlling climb and turn rates through roll and pitch commands to the inner-loop attitude controller (Beard and McLain, 2012). Turning is not achieved by controlling yaw angle or turn rate directly, but rather through banked-turn maneuvers.

The orientation, or *attitude*, of a fixed-wing aircraft relative to an inertial reference frame is represented, both globally and uniquely, by an element of the special orthogonal group SO(3), which is the set of 3 by 3 rotation matrices. The Euler angles given by roll, pitch and yaw provide a minimal, local coordinate system on SO(3), but will suffer from "gimbal-lock" singularities (Markley and Crassidis, 2014).

In the last decades, coordinate-free geometric attitude controllers, designed directly on SO(3), have been proposed in the literature, without the need for attitude parametrizations, and with no singularities (Chaturvedi et al., 2011). Another advantage of these approaches is that such controllers are often *geodesic* in the sense that proportional action is designed to steer the vehicle along the shortest path in the physical rotation space, whereas

controllers based on Euler angles are not. These advantages are desirable when the controlled vehicle is subject to large angle rotations, e.g. a UAV recovering from large attitude errors resulting from severe wind gusts (Johansen et al., 2014).

Controllers designed on SO(3), or using quaternions (Wen and Kreutz-Delgado, 1991), control the full attitude, and therefore can not be directly applied to fixed-wing aircraft using banked turn maneuvers. Instead of studying the full attitude, some authors consider a reduced-attitude representation, evolving on the two-sphere, $\mathbb{S}^2 \subset \mathbb{R}^3$ (Bullo et al., 1995). In this space of reduced attitude, all rotations that are related by a rotation about some fixed axis, are considered the same (Chaturvedi et al., 2009).

Control systems with reduced attitude evolving on $\mathbb{S}^2$ have previously been studied in the context of spin-axis stabilization of satellites (Bullo et al., 1995), pendulum stabilization (Chaturvedi et al., 2009), path-following control of underwater vehicles (Wrzos-Kaminska et al., 2019), control of multirotor UAVs (Casau et al., 2019) and for general rigid bodies (Mayhew and Teel, 2013).

In this paper, we present a smooth, nonlinear reduced-attitude controller for *fixed-wing* UAVs, in a coordinate-free manner, using a global, singularity-free attitude representation on $\mathbb{S}^2$. The chosen reduced-attitude representation is independent of the yaw angle and thus enables traditional banked-turn maneuvers. A consequence of this is that the presented approach fits directly into existing control architectures that rely on roll and pitch control in the inner loop. Also, no lateral/longitudinal decoupling assumptions are used in the design.

The reduced-attitude representation allows for a convenient decomposition of the dynamics and a natural corresponding decoupling of the control objective into two parts: 1. Reduced-attitude (roll/pitch) control, and 2. Control of the angular velocity about the inertial z-axis (turn rate control). Since only two control torques are needed to control the reduced attitude, there is one degree of freedom left to do turn rate control, which essentially performs turn coordination, providing damping about the inertial z-axis, and reducing the sideslip angle.

Almost semiglobal exponential tracking of reduced attitude is established using Lyapunov methods. In the special case of regulation, a stronger almost global asymptotic stability result is established. Because of topological constraints when dealing with compact manifolds (Bhat and Bernstein, 2000), the latter is the strongest possible stability result possible for continuous attitude control systems (Chaturvedi et al., 2011). Using hybrid control however, the region of attraction can be made global as shown in e.g. Mayhew and Teel (2013). Applications of hybrid methods to the attitude control of fixed-wing UAVs are explored further in our companion paper (Reinhardt et al., 2020).

2. PRELIMINARIES AND PROBLEM STATEMENT

2.1 Notation

The three-dimensional special orthogonal group is the set
$$\text{SO}(3) = \{R \in \mathbb{R}^{3\times3} \colon R^\top R = I_3, \det R = 1\}, \qquad (1)$$
where $I_3 \in \mathbb{R}^{3\times3}$ is the identity matrix. An element $R \in \text{SO}(3)$ is called a rotation matrix and transforms vectors from a body-fixed frame to an inertial reference frame.

For any $a, b \in \mathbb{R}^3$, the matrix $S(a) = -S^\top(a) \in \mathfrak{so}(3)$ is the skew-symmetric matrix such that $S(a)b = a \times b$. From properties of the cross product, $S(a)b = -S(b)a$ and $S(a)a = 0$.

The two-sphere $\mathbb{S}^2 \subset \mathbb{R}^3$ is defined by
$$\mathbb{S}^2 = \{x \in \mathbb{R}^3 \colon \|x\| = 1\}, \qquad (2)$$
where $\|x\| = \sqrt{x^\top x}$ is the Euclidean norm. The tangent space at a point $x \in \mathbb{S}^2$ can be identified with the vectors $v \in \mathbb{R}^3$ that are orthogonal to x:
$$\mathrm{T}_x\mathbb{S}^2 = \{v \in \mathbb{R}^3 \colon x \cdot v = 0\}, \qquad (3)$$
and the tangent bundle $\mathrm{T}\mathbb{S}^2$ is the set
$$\mathrm{T}\mathbb{S}^2 = \{(x,v) \colon x \in \mathbb{S}^2, v \in \mathrm{T}_x\mathbb{S}^2\}. \qquad (4)$$

The normal space $\mathrm{N}_x\mathbb{S}^2$ is the orthogonal complement of $\mathrm{T}_x\mathbb{S}^2$, given by the set of vectors parallel to x, or
$$\mathrm{N}_x\mathbb{S}^2 = \{w \in \mathbb{R}^3 \colon w \cdot v = 0 \text{ for all } v \in \mathrm{T}_x\mathbb{S}^2\}. \qquad (5)$$

Define the orthogonal and parallel projections $\Pi_x^\perp \colon \mathbb{R}^3 \to \mathrm{T}_x\mathbb{S}^2$ and $\Pi_x^\| \colon \mathbb{R}^3 \to \mathrm{N}_x\mathbb{S}^2$ by
$$\Pi_x^\perp = I_3 - xx^\top = -S^2(x), \qquad \Pi_x^\| = xx^\top. \qquad (6)$$
Then, any vector $v \in \mathbb{R}^3$ can be written as the sum $v = \Pi_x^\perp v + \Pi_x^\| v$.

Explicit time arguments will be used for state variables only when considering specific solutions, or for signals and functions in general when we want to highlight that time-varying exogenous signals are considered. At some points we will use a slight abuse of notation and write e.g. $V(t)$ for a Lyapunov function evaluated along system trajectories, when we really mean $V(x(t))$.

Lastly, the positive real numbers will be denoted $\mathbb{R}_+$, the set of 3 by 3 symmetric positive definite matrices will be denoted $\mathcal{P}_+^3$, and the maximum and minimum eigenvalues of a square matrix A will be denoted $\lambda_{\max}(A)$, $\lambda_{\min}(A)$, respectively.

2.2 UAV Attitude Dynamics

We will consider the following control-affine, fully actuated attitude dynamics for a fixed-wing UAV:
$$\dot{R} = RS(\omega) \qquad (7)$$
$$J\dot{\omega} = f(\omega, v_r, \delta_t) + G(\omega, v_r)u, \qquad (8)$$
where $\omega = [p \ q \ r]^\top \in \mathbb{R}^3$ is the body-fixed angular velocity, $J \in \mathcal{P}_+^3$ is the inertia matrix, $v_r = [v_{r_1} \ v_{r_2} \ v_{r_3}]^\top \in \mathbb{R}^3$ is the body-fixed (air) relative velocity, $\delta_t \in [0,1]$ is the throttle, and $u = [\delta_a \ \delta_e \ \delta_r]^\top$, where $\delta_a, \delta_e, \delta_r \in \mathbb{R}$ are the aileron, elevator and rudder control surface deflection angles, respectively.

Let $M_a(v_r, \omega)$ denote the aerodynamic moments that are independent of the control u, and $M_t(\delta_t)$ denote the reaction torque from the propeller. The drift term $f(\omega, v_r, \delta_t)$ can then be written as follows:
$$f(\omega, v_r, \delta_t) = S(J\omega)\omega + M_a(v_r, \omega) + M_t(\delta_t). \qquad (9)$$

Let the airspeed V_a, angle of attack α and sideslip angle β be defined by
$$V_a = \|v_r\| = \sqrt{v_{r_1}^2 + v_{r_2}^2 + v_{r_3}^2} \qquad (10)$$
$$\alpha = \text{atan2}\,(v_{r_1}, v_{r_3}), \qquad \beta = \text{atan2}\,(v_{r_2}, v_{r_1}), \qquad (11)$$
where $\text{atan2}(y,x)$ is the four-quadrant inverse tangent. Since V_a, α and β are functions of v_r, as a slight abuse of notation, the latter will be used as function argument for compactness.

Following Beard and McLain (2012), Stevens et al. (2016), the aerodynamic moment vector, and control effectiveness matrix $G(\omega, v_r)$ can be written in general form as
$$M_a(\omega, v_r) = \frac{1}{2}\rho V_a^2 S \begin{bmatrix} bC_l(\alpha, \beta, \omega) \\ cC_m(\alpha, \beta, \omega) \\ bC_n(\alpha, \beta, \omega) \end{bmatrix} \qquad (12)$$
$$G(\omega, v_r) = \frac{1}{2}\rho V_a^2 S \begin{bmatrix} bC_{l_u}(\alpha, \beta, \omega)^\top \\ cC_{m_u}(\alpha, \beta, \omega)^\top \\ bC_{n_u}(\alpha, \beta, \omega)^\top \end{bmatrix}, \qquad (13)$$
where $\rho, S, b, c \in \mathbb{R}_+$ is the density of air, the wing planform area, the wingspan and the aerodynamic chord, respectively. The functions C_l, C_m and C_n are roll, pitch and yaw moment coefficients, respectively, while the vector-valued functions C_{l_u}, C_{m_u} and C_{n_u} map control surface deflections to torques.

Assumption 1. The control effectiveness matrix $G(\omega, v_r)$ has full rank.

From (13), it is clear that a consequence of this assumption is that a strictly positive airspeed is required, i.e. $V_a \geq \underline{V}_a$ for some $\underline{V}_a \in \mathbb{R}_+$.

Remark 1. For common parametrizations based on constant control effectiveness coefficients (Beard and McLain, 2012; Stevens et al., 2016), it can be shown that the full rank condition corresponds to *primary control* coefficients being larger than the coefficients associated with *secondary* roll-yaw coupling effects. The full rank assumption is therefore reasonable for most common fully actuated control surface configurations.

Throughout the text, the throttle δ_t and relative velocity v_r, and therefore also α, β and V_a (as functions of v_r), will be treated as known time-varying input signals.

Remark 2. Note that since the translational subsystem (see Stevens et al. (2016)) depends on R, ω and u, the relative velocity v_r is not truly an exogenous signal. Nevertheless, as a decoupling maneuver, we will assume that it is a known signal available for feedback. This should be considered when integrating the control system developed in this paper in UAV GNC systems, e.g. using bandwidth separation.

2.3 Reduced Attitude

Let $e_3 = [0\ 0\ 1]^\top$ be fixed in the inertial frame. Transforming e_3 to the body-fixed frame gives the reduced-attitude vector $\Gamma \in \mathbb{S}^2$ defined by

$$\Gamma = R^\top e_3. \qquad (14)$$

This particular choice of reduced-attitude representation has been applied to stabilized the inverted equilibrium manifold of the 3-D pendulum in Chaturvedi et al. (2009), and corresponds to the direction of gravitational acceleration, expressed in the body-fixed frame, and is thus invariant to rotations about the inertial z-axis. The latter can be seen by expanding (14) using the roll-pitch-yaw Euler angle parametrization:

$$\Gamma = [-\sin(\theta)\ \cos(\theta)\sin(\phi)\ \cos(\theta)\cos(\phi)]^\top, \qquad (15)$$

where $\phi \in [-\pi, \pi]$ is the roll angle, and $\theta \in [-\pi/2, \pi/2]$ is the pitch angle.

Using (6), we can perform an orthogonal decomposition of the angular velocity ω with respect to Γ such that $\omega = \omega^\perp + \omega^\|$, where

$$\omega^\perp \triangleq \Pi_\Gamma^\perp \omega \in T_\Gamma \mathbb{S}^2 \qquad \omega^\| \triangleq \Pi_\Gamma^\| \omega \in N_\Gamma \mathbb{S}^2. \qquad (16)$$

Differentiating (14) using (7) gives

$$\dot{\Gamma} = \Gamma \times \omega = \Gamma \times \omega^\perp \in T_\Gamma \mathbb{S}^2. \qquad (17)$$

The parallel component $\omega^\|$ is the angular velocity about the inertial z-axis (expressed in the body-fixed frame), and clearly does not influence $\dot{\Gamma}$.

Differentiating (16) and using (17) gives

$$\dot{\omega}^\perp = \Pi_\Gamma^\perp \dot{\omega} + \omega^\perp \times \omega^\| \qquad (18)$$

$$\dot{\omega}^\| = \Pi_\Gamma^\| \dot{\omega} + \omega^\| \times \omega^\perp, \qquad (19)$$

where we have also applied the identity $a^\top S a = 0$ for any $a \in \mathbb{R}^3$ and $S \in so(3)$.

2.4 Reference System

Let a time-varying reduced-attitude reference vector $\Gamma_d(t) \in \mathbb{S}^2$ satisfy

$$\dot{\Gamma}_d = \Gamma_d \times \omega_d, \qquad (20)$$

where $\omega_d \in T_{\Gamma_d}\mathbb{S}^2$. We will assume that the desired angular velocity is uniformly bounded, i.e. $\|\omega_d\| \leq B$, and that $\dot{\omega}_d$ is continuous.

Consider the projection of ω_d onto the tangent space $T_\Gamma \mathbb{S}^2$, given by $\Pi_\Gamma^\perp \omega_d \in T_\Gamma \mathbb{S}^2$. Using (6), (17) and the fact that $a^\top S(b)c = b^\top S(c)a = c^\top S(a)b$ for any $a, b, c \in \mathbb{R}^3$, the derivative can be found to satisfy

$$\frac{d}{dt}(\Pi_\Gamma^\perp \omega_d) = \Pi_\Gamma^\perp \dot{\omega}_d + \omega^\perp \times \Pi_\Gamma^\| \omega_d + \Pi_\Gamma^\|(\omega_d \times \omega^\perp). \qquad (21)$$

2.5 Potential Function

Let a smooth configuration error function $\Psi: \mathbb{S}^2 \times \mathbb{S}^2 \to \mathbb{R}$ be defined by

$$\Psi(\Gamma, \Gamma_d) = \frac{1}{2}\|\Gamma - \Gamma_d\|^2 = 1 - \Gamma_d \cdot \Gamma. \qquad (22)$$

The function Ψ measures the "distance" between two points Γ and Γ_d on $\mathbb{S}^2$, and is clearly positive definite with respect to $\Gamma = \Gamma_d$. There are two critical points: A minimum when $\Gamma = \Gamma_d$, and a maximum when $\Gamma = -\Gamma_d$. In subsequent Lyapunov analysis, Ψ will be used as pseudo-potential energy. When Γ_d is constant, we write $\Psi(\Gamma)$ and also remove Γ_d as an argument of the corresponding Lyapunov function.

2.6 Error States

To design proportional feedback on $\mathbb{S}^2$, let a configuration error vector $e_\Gamma: \mathbb{S}^2 \times \mathbb{S}^2 \to T_\Gamma \mathbb{S}^2$ be given by

$$e_\Gamma = \Gamma \times \Gamma_d, \qquad (23)$$

and define the angular velocity error as

$$e_\omega = \omega^\perp - \Pi_\Gamma^\perp \omega_d = \Pi_\Gamma^\perp(\omega - \omega_d) \in T_\Gamma \mathbb{S}^2. \qquad (24)$$

From (18) and (21), the derivative of e_ω can be written as

$$\dot{e}_\omega = \Pi_\Gamma^\perp\left(\dot{\omega} - \dot{\omega}_d + \omega^\perp \times (\omega^\| - \Pi_\Gamma^\| \omega_d)\right) - \Pi_\Gamma^\|(\omega_d \times e_\omega). \qquad (25)$$

The error vector e_Γ can be viewed as a gradient vector field on $\mathbb{S}^2$ induced by the potential function Ψ (Lee et al., 2011), and it vanishes at the critical points of Ψ. The error terms e_Γ and e_ω are also compatible in the sense that $\dot{\Psi} = e_\omega^\top e_\Gamma$, which will cancel with the proportional feedback term defined later when calculating the derivative of a Lyapunov function. The error vector e_Γ is geodesic in the sense that its direction defines an axis of rotation which connects Γ and Γ_d with the shortest possible curve on $\mathbb{S}^2$.

Remark 3. Other configuration error vectors (with corresponding potential functions) on $\mathbb{S}^2$ could be used in place of (23), without changing the general approach considered in this paper. For instance, alternative error vectors that do not vanish when approaching $-\Gamma_d$ (at the cost of being undefined at this point) can be found in Bullo et al. (1995), Chaturvedi and McClamroch (2009) and Ramp and Papadopoulos (2015).

2.7 Control Objective

Let an orthogonal decomposition of the control input vector u be given by $u = u^\perp + u^\|$, where $J^{-1}G(\omega, v_r)u^\perp \in T_\Gamma \mathbb{S}^2$, and $J^{-1}G(\omega, v_r)u^\| \in N_\Gamma \mathbb{S}^2$.

The control objective can be stated as follows:

Reduced-Attitude Tracking. Design a state-feedback control law $u^\perp$ such that $\Gamma(t) \to \Gamma_d(t)$ and $e_\omega(t) \to 0$ as $t \to \infty$.

A special case of reduced-attitude tracking is the case when Γ_d is constant, so $\omega_d = 0$ and $e_\omega = \omega^\perp$. We can formulate the following regulation problem:

Reduced-Attitude Regulation. Design a state-feedback control law $u^\perp$ such that $\Gamma(t) \to \Gamma_d$ constant and $\omega^\perp(t) \to 0$ as $t \to \infty$.

The remaining degree of freedom provided by $u^\|$ is in the nullspace of the orthogonal projection and as such does not interfere with the control of reduced attitude. It should be used for turn coordination and to stabilize the parallel component of angular velocity.

3. MAIN RESULT

This section introduces the main result for reduced-attitude tracking control for fixed-wing UAVs, where a control law $u^\perp$ is given. The design of a control law using the remaining degree of freedom, given by $u^\|$ is treated in Section 4.

Proposition 1. (Reduced-Attitude Tracking). Consider the reduced-attitude error dynamics defined by (8), (17), and (25), assuming $V_a \geq \underline{V_a} > 0$ and that the control effectiveness matrix $G(\omega, v_r)$ has full rank. With $k_p \in \mathbb{R}_+$ and $K_d \in \mathcal{P}_+^3$, let a smooth tracking control law $u^\perp$ satisfying $J^{-1}G(\omega, v_r)u^\perp \in T_\Gamma \mathbb{S}^2$ be given by

$$u^\perp = G^{-1}(\omega, v_r)J\bigg(-k_p e_\Gamma - \Pi_\Gamma^\perp K_d e_\omega$$
$$- \Pi_\Gamma^\perp J^{-1} f(\omega, v_r, \delta_t) - \omega^\perp \times (\omega^\| - \Pi_\Gamma^\| \omega_d) + \Pi_\Gamma^\perp \dot{\omega}_d \bigg). \tag{26}$$

With δ_t, v_r treated as bounded, time-varying exogenous signals, the closed-loop error system has two equilibrium solutions given by $(\Gamma, e_\omega) = (\pm \Gamma_d, 0)$. The desired equilibrium $(\Gamma_d, 0)$ is exponentially stable, with region of exponential convergence given by

$$\Psi(\Gamma(0), \Gamma_d(0)) \leq \overline{\Psi} \tag{27}$$
$$\|e_\omega(0)\| \leq \sqrt{2k_p \left(\overline{\Psi} - \Psi(\Gamma(0), \Gamma_d(0)) \right)}, \tag{28}$$

for some $\overline{\Psi} < 2$, where 2 is the maximum value of Ψ, attained at $\Gamma = -\Gamma_d$. The additional undesired equilibrium $(-\Gamma_d, 0)$ is unstable.

Additionally, if $\omega_d = 0$, the desired equilibrium $(\Gamma_d, 0)$ is almost globally asymptotically stable.

Proof. See Appendix A.

For almost all $\Psi(\Gamma(t_0), \Gamma_d(t_0)), e_\omega(t_0)$ (excluding $\Gamma(t_0) = -\Gamma_d(t_0)$), some k_p can be chosen such that (27), (28) is satisifed. The equilibrium $(\Gamma_d, 0)$ is therefore said to be *almost semiglobally exponentially stable* (Lee, 2015).

Remark 4. By exploiting passivity-properties in the Lyapunov design, the term $-\omega^\perp \times (\omega^\| - \Pi_\Gamma^\| \omega_d)$ in (26) could be replaced by $-\Pi_\Gamma^\perp \omega_d \times (\omega^\| - \Pi_\Gamma^\| \omega_d)$, without changing $\dot{V}$. This would also remove the seemingly unneeded cross

product term in (29). However, this would give a closed-loop system that depends on $\omega^\|$, and invalidate several arguments used in the proof.

Remark 5. A notable property of the control law (26) is that since the control effectiveness matrix $G(\omega, v_r)$ given by (13) contains a factor of V_a^2, the inverse matrix $G^{-1}(\omega, v_r)$ contains a factor of $1/V_a^2$. This means that the control law includes airspeed scaling. Also note that instead of compensating for the entire drift term $f(\omega, v_r, \delta_t)$, only the orthogonal projection is compensated for.

Parts of the proof is inspired by Lee (2016), where a tracking controller for a double integrator system on $\mathbb{S}^2$ is presented. However, Lee (2016) considers an inertial frame representation of reduced attitude, as opposed to (14), which is defined in the body-fixed frame. Also, no dynamics, or parallel component of the angular velocity is considered. In addition to compensating for the dynamics, compared to Lee (2016), the controller (26) allows a matrix gain K_d, projects the feedforward term $\dot{\omega}_d$ to $T_\Gamma \mathbb{S}^2$, and adds an additional term $-\omega^\perp \times \omega^\|$ to compensate for the "coriolis" term that appears when $\omega^\|$ is nonzero.

In the special case of regulation, where $\omega_d = 0$, and $e_\omega = \omega^\perp$, the control law (26) reduces to

$$u^\perp = G^{-1}(\omega, v_r)J\bigg(-k_p e_\Gamma - \Pi_\Gamma^\perp K_d \omega^\perp$$
$$- \Pi_\Gamma^\perp J^{-1} f(\omega, v_r, \delta_t) - \omega^\perp \times \omega^\| \bigg). \tag{29}$$

The closed-loop system in this case is autonomous. This means that LaSalle's invariance theorem (Khalil, 2002) can be applied. Inspired by the methodology presented for the 3-D pendulum in Chaturvedi et al. (2009), this can be combined with local analysis of the linearized closed-loop dynamics at the equilibria to show almost global asymptotic stability. However, the linearized dynamics in Chaturvedi et al. (2009) evolve on $\mathbb{R}^5$, since the state space includes the full angular velocity ω. In Lee et al. (2011), a closed-loop 3-D pendulum system is analyzed, with angular velocity in $T_\Gamma \mathbb{S}^2$ and with linearization evolving on $\mathbb{R}^4$, but only for very specific numerical values of the controller gains. The proof of almost global asymptotic stability follows Chaturvedi et al. (2009), but is adjusted to use a linearization on $\mathbb{R}^4$ instead of $\mathbb{R}^5$, inspired by Lee et al. (2011), but done in full generality. In addition, a matrix gain K_d is used instead of a scalar.

4. TURN COORDINATION

The control law defined by (26) does not inject damping about the axis defined by Γ. The control $u^\|$ can be utilized to do this. Let a reference for the angular velocity about the vertical axis of the inertial frame be given by the equation for a coordinated turn with zero sideslip (Beard and McLain, 2012):

$$\omega_d^\| = \dot{\psi}_d \Gamma, \qquad \dot{\psi}_d = \frac{g}{V_a} \tan(\phi). \tag{30}$$

Note that care needs to be taken to avoid the singularity at $\Gamma_3 = 0$, corresponding to $\phi = \pm \pi/2$, either by constraining the value of ϕ used in (30), or by using the reference instead. A controller that adds damping about Γ without

interfering with the banked turn manuever is then given by

$$u^{\parallel} = G^{-1}(\omega, v_r)J\left(-k_{tc}(\omega^{\parallel} - \omega_d^{\parallel}) - \Pi_{\Gamma}^{\parallel}J^{-1}f(\omega, v_r, \delta_t)\right), \tag{31}$$

where $k_{tc} \in \mathbb{R}_+$ is a scalar design parameter.

As an alternative to (31), for some $k_{\beta} \in \mathbb{R}_+$, consider the following control law, which is designed to drive the sideslip angle to zero:

$$u^{\parallel} = G^{-1}(\omega, v_r)J\,\Pi_{\Gamma}^{\perp}(k_{\beta}\beta e_3). \tag{32}$$

5. COMPARISON WITH CONTROLLER BASED ON EULER ANGLES

In this section, the geometric controller presented in Section 3 will be compared to a controller based on Euler angles. For $K_{\omega} \in \mathcal{P}_+^3$, consider the cascaded dynamic inversion based controller

$$u = G^{-1}(\omega, v_r)J\left(-K_{\omega}(\omega - \bar{\omega}_d) - J^{-1}f(\omega, v_r, \delta_t)\right), \tag{33}$$

where the bar in $\bar{\omega}_d$ is introduced to distinguish it from ω_d in (20). The desired angular velocity is computed using (30) and linear state feedback from the roll and pitch regulation errors $\tilde{\phi} \triangleq \phi - \phi_d$, $\tilde{\theta} \triangleq \theta - \theta_d$ as follows:

$$\bar{\omega}_d = T^{-1}(\phi, \theta)\begin{bmatrix} -k_{\phi}\tilde{\phi} \\ -k_{\theta}\tilde{\theta} \\ \frac{g}{V_a}\tan(\phi) \end{bmatrix} \tag{34}$$

where $k_{\phi}, k_{\theta} \in \mathbb{R}_+$, and $T^{-1}(\phi, \theta)$ is the inverse of the Euler angle transformation matrix, given by (Beard and McLain, 2012)

$$T^{-1}(\phi, \theta) = \begin{bmatrix} 1 & 0 & -\sin(\theta) \\ 0 & \cos(\phi) & \cos(\theta)\sin(\phi) \\ 0 & -\sin(\phi) & \cos(\theta)\cos(\phi) \end{bmatrix} \tag{35}$$

for $\theta \neq \pm\pi/2$. Note that the third column is Γ (see (15)).

Remark 6. Apart from the dynamic inversion term, this controller has similar structure as the control architecture used in the PX4 open source autopilot (Meier et al., 2015).

To compare the geometric controller from Section 3 with the Euler angle controller (33)-(35), we consider the regulation case with $\omega_d = 0$, and set $K_d = K_{\omega} = k_d I_3$, $k_{\theta} = k_{\phi} = k_p/k_d$, and (31) is used for $u^{\parallel}$ with $k_{tc} = k_d$.

For the geometric controller, the closed-loop angular velocity dynamics then become

$$\dot{\omega} = -k_p e_{\Gamma} - k_d\omega + k_d\omega_d^{\parallel}, \tag{36}$$

while for the controller based on Euler angles, the closed-loop dynamics are

$$\dot{\omega} = -k_p e_{\theta\phi} - k_d\omega + k_d\omega_d^{\parallel}, \tag{37}$$

where we have introduced the following error vector:

$$e_{\theta\phi} \triangleq \begin{bmatrix} \tilde{\phi} & \frac{k_{\theta}}{k_{\phi}}\tilde{\theta}\cos(\phi) & -\frac{k_{\theta}}{k_{\phi}}\tilde{\theta}\sin(\phi) \end{bmatrix}^{\top}. \tag{38}$$

The only difference between (36) and (37) lies in the proportional error vectors. By calculating $\Gamma \cdot e_{\theta\phi} = -\tilde{\phi}\sin(\theta) \neq 0$, we see that $e_{\theta\phi} \notin \mathrm{T}_{\Gamma}\mathbb{S}^2$, so the proportional action has a different direction than the geodesic direction defined by e_{Γ}. The error vectors also have different magnitude, but this can be changed using a different potential
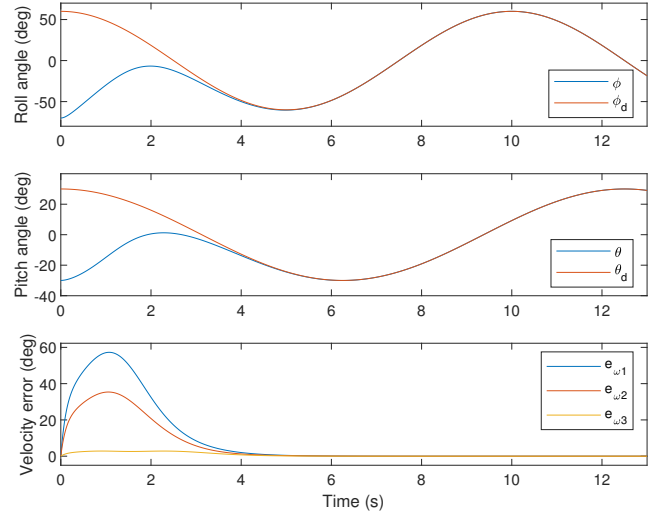

Fig. 1. Tracking scenario: Roll, pitch and angular velocity error.

function (see Remark 3). In the numerical simulation study of Section 6 we will normalize the magnitude of the error vectors by redefining e_{Γ} as $e_{\Gamma}' = \|e_{\theta\phi}\| \cdot e_{\Gamma}/\|e_{\Gamma}\|$, which enables us to compare the controllers on equal grounds.

6. NUMERICAL EXAMPLE

This section presents some simulation results using a model of the Aerosonde UAV (Beard and McLain, 2012) with a simple PI controller for airspeed and a constant reference of $35\,\mathrm{m/s}$. In the tracking example, (32) is used for $u^{\parallel}$, while (31) is used in the regulation case. The angular velocity is initialized to zero in both cases, while the controller parameters are set to $k_p = 9.5$, $K_d = 8I$ and $k_{\beta} = 10$.

6.1 Tracking

Consider a tracking scenario, where a trajectory $(\Gamma_d(t), \omega_d(t), \dot{\omega}_d(t))$ has been generated using (15), $\phi_d(t) = 60\frac{\pi}{180}\cos(0.1 \cdot 2\pi t)$, $\theta_d(t) = 30\frac{\pi}{180}\cos(0.08 \cdot 2\pi t)$ and their analytical first and second order derivatives. Initial reduced attitude is set using $\phi(0) = -70°$ and $\theta(0) = -30°$. Fig. 1 shows that reduced attitude, visualized using roll and pitch angles, converge to the desired trajectory from large initial errors, while the angular velocity error goes to zero. Angle of attack, sideslip and control surface deflection angles, which attain reasonable values throughout the maneuver, are displayed in Fig. 2.

6.2 Regulation

Now consider a regulation case, where $\omega_d = 0$. The constant reference is generated using $\phi_d = 60°$ and $\theta_d = 30°$. Initial roll and yaw angles are set to zero, while $\theta(0)$ is calculated using a trim routine. As explained in Section 5, the magnitude of the error vector (23) is scaled for comparison with the Euler angle controller. Fig. 3 shows that the UAV performs a banked turn maneuver with approximately constant turn rate, and roll and pitch angles converge in both cases. For this specific manuever, the geometric controller seem to have
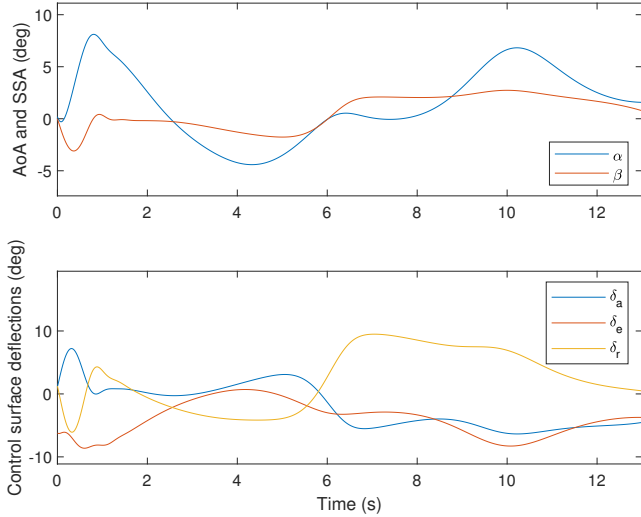
Fig. 2. Tracking scenario: Angle of attack (AoA), sideslip angle (SSA) and control surface deflection angles.
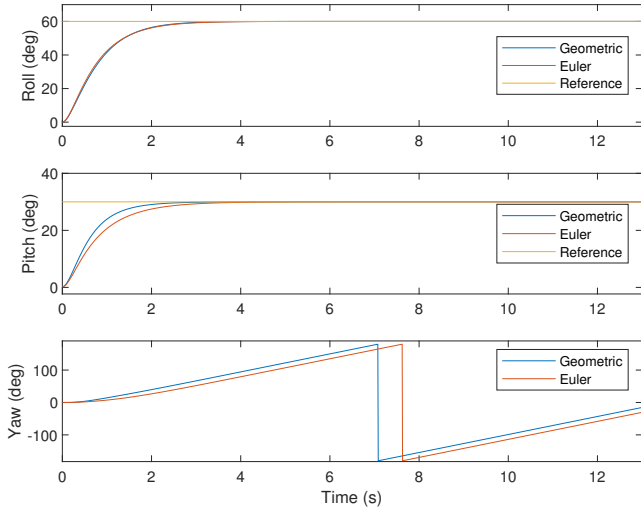

Fig. 3. Regulation scenario: Euler angle comparison.
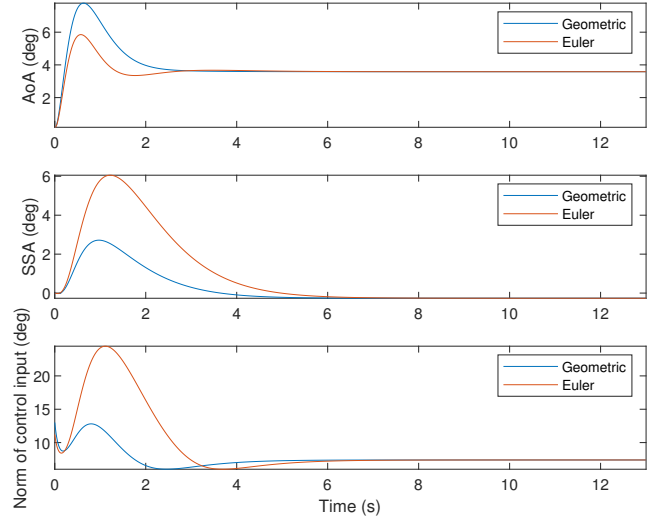

Fig. 4. Regulation scenario: Angle of attack, sideslip angle and norm of control input.

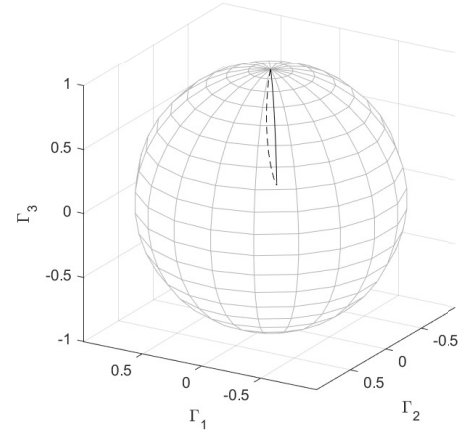Fig. 5. Regulation scenario: Trajectories on the two-sphere. Solid: Geometric controller. Dashed: Controller based on Euler angles.

a slightly faster response in pitch. The difference can be more clearly understood by looking at Fig. 5. The response of the geometric controller is shown to make the UAV take the shortest path between Γ and Γ_d, while the controller based on Euler angles does not. Fig. 4 might indicate that this makes the geometric controller spend less control energy. However, the sideslip angle is smaller, which also reduces the magnitude of the compensated drift term $f(\omega, v_r, \delta_t)$. Further investigation should compare the two controllers when $f(\omega, v_r, \delta_t)$ is unknown, and integral action is implemented.

Appendix A. PROOF OF PROPOSITION 1

A.1 Equilibrium Points

Differentiating (23), applying the identity $S(a)S(b) - S(b)S(a) = S(S(a)b)$ and combining with (8), (25), (26) gives the non-autonomous closed-loop error system

$$\dot{e}_\Gamma = -S(\omega_d)e_\Gamma - S(\Gamma_d)S(\Gamma)e_\omega \tag{A.1}$$

$$\dot{e}_\omega = -k_p e_\Gamma - \Pi_\Gamma^\perp K_d e_\omega - \Pi_\Gamma^\parallel (\omega_d \times e_\omega), \tag{A.2}$$

which gives the equilibrium condition

$$\begin{bmatrix} -S(\omega_d) & -S(\Gamma_d)S(\Gamma) \\ -k_p I_3 & -S^2(\Gamma)K_d S^2(\Gamma) - \Gamma\Gamma^\top S(\omega_d) \end{bmatrix} \begin{bmatrix} e_\Gamma \\ e_\omega \end{bmatrix} = \begin{bmatrix} 0 \\ 0 \end{bmatrix}, \tag{A.3}$$

where we have used the fact that $-S^2(\Gamma)e_\omega = e_\omega$. For (A.3) to be satisfied for all t, where the time-dependence is implicit through $\Gamma_d(t), \omega_d(t)$, we get $e_\Gamma = e_\omega = 0$. Note that, when $\omega_d = 0$, the matrix above is rank-deficient, with $v = [0 \ w]^\top$ as a basis of the nullspace, where w is parallel to Γ. But e_ω lies in $T_\Gamma\mathbb{S}^2$. Thus, equilibrium solutions are given by $(\Gamma, e_\omega) = (\pm\Gamma_d, 0)$.

A.2 Exponential Tracking

Consider the Lyapunov-like function $V \colon T\mathbb{S}^2 \times \mathbb{S}^2 \to \mathbb{R}_{\geq 0}$

$$V_1(\Gamma, e_\omega, \Gamma_d) = k_p \Psi(\Gamma, \Gamma_d) + \frac{1}{2}e_\omega^\top e_\omega. \tag{A.4}$$

Differentiating along closed-loop trajectories of (A.2) gives

$$\dot{V}_1 = k_p e_\omega^\top e_\Gamma + e_\omega^\top \left(-k_p e_\Gamma - \Pi_\Gamma^\perp K_d e_\omega - \Pi_\Gamma^\parallel (\omega_d \times e_\omega) \right) \tag{A.5}$$

$$= -e_\omega^\top K_d e_\omega \leq -\lambda_{\min}(K_d)\|e_\omega\|^2 \leq 0, \tag{A.6}$$

where the last term in (A.5) disappears since $e_\omega \in T_\Gamma \mathbb{S}^2$, and we have used the property $e_\omega^\top \Pi_\Gamma^\perp = (\Pi_\Gamma^\perp e_\omega)^\top = e_\omega$. For initial conditions satisfying (27), (28), we get $V_1(t_0) \leq k_p \overline{\Psi}$. Since $V_1(t)$ is non-increasing, we get:

$$k_p \Psi(\Gamma(t), \Gamma_d(t)) \leq V_1(t) \leq V_1(t_0) \leq k_p \overline{\Psi}, \tag{A.7}$$

which means that $\Psi(\Gamma(t), \Gamma_d(t)) \leq \overline{\Psi}$. For the sublevel set $L_2 = \left\{ \Gamma, \Gamma_d \in \mathbb{S}^2 : \Psi(\Gamma, \Gamma_d) \leq \overline{\Psi} \right\}$, we can bound Ψ by

$$\frac{1}{2}\|e_\Gamma\|^2 \leq \Psi(\Gamma, \Gamma_d) \leq \frac{1}{2 - \overline{\Psi}}\|e_\Gamma\|^2. \tag{A.8}$$

Now, consider the Lyapunov function candidate

$$V_2(\Gamma, e_\omega, \Gamma_d) = V_1 + c e_\omega^\top e_\Gamma. \tag{A.9}$$

Using (A.8), we can derive upper and lower bounds

$$\frac{1}{2} z^\top M_1 z \leq V_2 \leq \frac{1}{2} z^\top M_2 z, \tag{A.10}$$

where $z = [\|e_\Gamma\| \ \|e_\omega\|]^\top$ and

$$M_1 = \begin{bmatrix} k_p & -c \\ -c & 1 \end{bmatrix}, \qquad M_2 = \begin{bmatrix} \dfrac{2k_p}{2 - \overline{\Psi}} & c \\ c & 1 \end{bmatrix}. \tag{A.11}$$

Differentiating V_2 along the closed-loop trajectories gives

$$\dot{V}_2 = -e_\omega^\top K_d e_\omega + c\dot{e}_\omega^\top e_\Gamma + c e_\omega^\top \dot{e}_\Gamma. \tag{A.12}$$

The cross terms can be bounded as follows:

$$\|e_\omega^\top \dot{e}_\Gamma\| \leq \|e_\omega\| \|\omega_d\| \|e_\Gamma\| + \|e_\omega\|^2 \leq B\|e_\omega\|\|e_\Gamma\| + \|e_\omega\|^2 \tag{A.13}$$

$$\|e_\Gamma^\top \dot{e}_\omega\| \leq -k_p\|e_\Gamma\|^2 + \lambda_{\max}(K_d)\|e_\Gamma\|\|e_\omega\|, \tag{A.14}$$

which leads to

$$\dot{V}_2 = -e_\omega^\top K_d e_\omega + c\dot{e}_\omega^\top e_\Gamma + c e_\omega^\top \dot{e}_\Gamma \leq -z^\top M_3 z, \tag{A.15}$$

where the matrix M_3 is given by

$$M_3 = \begin{bmatrix} c k_p & -\dfrac{c\left(B + \lambda_{\max}(K_d)\right)}{2} \\ -\dfrac{c\left(B + \lambda_{\max}(K_d)\right)}{2} & \lambda_{\min}(K_d) - c \end{bmatrix} \tag{A.16}$$

If c is chosen to satisfy

$$c < \min\left\{ \sqrt{k_p}, \ \frac{4k_p \lambda_{\min}(K_d)}{4k_p + (B + \lambda_{\max}(K_d))^2} \right\}, \tag{A.17}$$

then M_1, M_2 and M_3 are all positive definite.

By following similar arguments as in the proof of Theorem 4.10 in Khalil (2002), we get that $V_2(t)$ and $\|z(t)\|$ converges exponentially to zero, which in turn means that $(\Gamma(t), e_\omega(t))$ converges exponentially to $(\Gamma_d(t), 0)$, with the region of exponential convergence given by (27) and (28).

A.3 Instability of Undesired Equilibrium

To show that the undesired equilibrium is unstable, define

$$W = 2k_p - V_2 \geq -\frac{1}{2}\|e_\omega\|^2 - c\|e_\omega\|\|e_\Gamma\| + k_p(2 - \Psi(\Gamma, \Gamma_d)). \tag{A.18}$$

At the undesired equilibrium $(-\Gamma_d, 0)$, we have $W = 0$, and $\dot{W} = -\dot{V}_2$ is positive definite from (A.15). Now

consider Γ arbitrarily close to $-\Gamma_d$. In this case, the term $2 - \Psi(\Gamma, \Gamma_d)$ is positive, and we can choose $\|e_\omega\|$ sufficiently small such that $W > 0$ and $\dot{W} > 0$. By Theorem 4.3 in Khalil (2002), the equilibrium $(-\Gamma_d, 0)$ is unstable.

A.4 Almost Global Regulation

When $\omega_d = 0$, (A.6) reduces to $\dot{V}_1 = -(\omega^\perp)^\top K_d \omega^\perp \leq 0$, so the set given by

$$\Omega \triangleq \{(\Gamma, \omega^\perp) \in \mathbb{S}^2 \times T_\Gamma \mathbb{S}^2 : \\ V_1(\Gamma(t), \omega^\perp(t)) \leq V_1(\Gamma(t_0), \omega^\perp(t_0))\} \tag{A.19}$$

is positively invariant. Since $\mathbb{S}^2$ is compact, all sublevel sets of V_1 are compact, which means that the set Ω is compact. Let E be set of points in Ω where $\dot{V}_1 = 0$. In E, $\omega^\perp = 0$, which when inserted into (A.2) and using (23) leads to $\Gamma = \pm \Gamma_d$. By Theorem 4.4 in Khalil (2002) (LaSalle), every solution starting in Ω then converges asymptotically to one of the equilibrium solutions $(\pm \Gamma_d, 0)$. Local asymptotic stability of the desired equilibrium point, as well as the instability of the undesired equilibirum follows from Sections A.2 and A.3. To establish almost global asymptotic stability of the desired equilibrium we will study the local structure of the undesired equilibrium.

Let a perturbation of the equilibrium solution $(\Gamma(t), \omega^\perp(t)) = (\Gamma_e, 0)$ be given in terms of a perturbation parameter ϵ as $(\Gamma_\epsilon(t, \epsilon), \omega_\epsilon^\perp(t, \epsilon)) = (e^{-\epsilon S(\eta(t))}\Gamma_e, \epsilon \delta\omega(t))$, which satisfies $\eta(t) \cdot \Gamma_e = \delta\omega(t) \cdot \Gamma_e = 0$ for all t. Now, consider the perturbed equations of motion (17), (A.2) given by

$$\dot{\Gamma}_\epsilon(t, \epsilon) = \Gamma_\epsilon(t, \epsilon) \times \omega_\epsilon^\perp(t, \epsilon) \tag{A.20}$$

$$\dot{\omega}_\epsilon^\perp(t, \epsilon) = -k_p \Gamma_\epsilon(t, \epsilon) \times \Gamma_d - K_d \omega_\epsilon^\perp(t, \epsilon) \\ + \Gamma_\epsilon(t, \epsilon)\Gamma_\epsilon^\top(t, \epsilon)K_d \omega_\epsilon^\perp(t, \epsilon). \tag{A.21}$$

Differentiating both sides with respect to ϵ and inserting $\epsilon = 0$ gives the linearized set of equations $\dot{x} = A(\Gamma_e)x$, where $x = [\eta \ \delta\omega]^\top$. For $\Gamma_e = -\Gamma_d$, we get

$$A(-\Gamma_d) \triangleq A = \begin{bmatrix} 0 & I_3 \\ -k_p S^2(\Gamma_d) & -S^2(\Gamma_d)K_d S^2(\Gamma_d) \end{bmatrix}, \tag{A.22}$$

where the relation $-S^2(\Gamma_d)\delta\omega = \delta\omega$ has been used to add the last factor in the lower right element of the matrix.

The state space has dimension six, but in reality, the system evolves on a four-dimensional subspace according to the constraints

$$Cx = \begin{bmatrix} \Gamma_e^\top & 0 \\ 0 & \Gamma_e^\top \end{bmatrix} \begin{bmatrix} \eta \\ \delta\omega \end{bmatrix} = \begin{bmatrix} 0 \\ 0 \end{bmatrix}, \tag{A.23}$$

which is respected by the linearized dynamics, in the sense that $CA = 0$.

If decomposing eigenvectors v_i of A into $v_i = [v_{i1}^\top \ v_{i2}^\top]^\top$, it follows from the equation $Av = \lambda v$ that eigenvalue-eigenvector pairs of A need to satisfy

$$v_{i2} = \lambda_i v_{i1} \tag{A.24}$$

$$-k_p S^2(\Gamma_d)v_{i1} - S^2(\Gamma_d)K_d S^2(\Gamma_d)v_{i2} = \lambda_i v_{i2}. \tag{A.25}$$

Inserting (A.24) into (A.25) and pre-multiplying with the complex conjugate transpose $\bar{v}_{i1}^\top$ of v_{i1} gives

$$a\lambda^2 + b\lambda - c = 0, \tag{A.26}$$

where

$$a = \bar{v}_{i1}^\top v_{i1} > 0 \qquad (A.27)$$

$$b = \bar{v}_{i1}^\top [-S^2(\Gamma_d)] K_d [-S^2(\Gamma_d)] v_{i1} \geq 0 \qquad (A.28)$$

$$c = k_p \bar{v}_{i1}^\top [-S^2(\Gamma_d)] v_{i1} \geq 0, \qquad (A.29)$$

since the matrix $-S^2(\Gamma_d)$ is positive semi-definite. The coefficients b and c are only (simultaneously) zero when $-S^2(\Gamma_d)v_{i1} = 0$, i.e. when v_{i1} has the form $v_{i1} = z_1\Gamma_d$ for some $z_1 \in \mathbb{C}$. In this case, (A.26) reduces to $a\lambda^2 = 0$, so $\lambda_1 = 0$ is an eigenvalue of A with algebraic multiplicity two, corresponding to the eigenvector $v_1 = [z_1\Gamma_d^\top \ \ 0^\top]^\top$. However, since A has rank five, the geometric multiplicity of λ_1 is one. To get a full Jordan basis, we choose the generalized eigenvector $v_2 = [z_2\Gamma_d^\top \ \ z_1\Gamma_d^\top]^\top$, which satisfies $(A - \lambda_1 I)v_2 = Av_2 = v_1$, for $z_2 \in \mathbb{C}$.

The solutions of the linearized system defined by (A.22) can be written in terms of its Jordan form as

$$x(t) = c_1 e^{\lambda_1 t} v_1 + c_2 e^{\lambda_1 t}(v_1 t + v_2) + \sum_{i=3}^{6} c_i h_i(t), \quad (A.30)$$

where the functions $h_i(t)$ depend on the vectors v_j, $j \in \{1, \ldots, 6\}$, the eigenvalues λ_k, $k = \{2,3,4,5\}$ and their multiplicities. The constants c_i depend on the intial condition $x(0) = \sum_{i=1}^{6} c_i v_i$, which satisifies $Cx(0) = 0$. Since the vectors v_1, v_2 do not satisfy the constraints (A.23), $c_1 = c_2 = 0$, so the solution $x(t)$ does not depend on λ_1.

Since $A \in \mathbb{R}^{6\times 6}$ is a rank five matrix, we know that no other eigenvectors are parallel to v_1, so for all remaining eigenvector pairs, $a, b, c > 0$. Since (A.26) has two solutions, we know from the quadratic formula that from the remaining eigenvalues λ_k, $k = \{2,3,4,5\}$, two are positive, and two are negative. This confirms that the undesired equilibrium point $(\Gamma, \omega^\perp) = (-\Gamma_d, 0)$ is unstable. Moreover, the stable eigenspace corresponding to the two negative eigenvalues is the tangent space to a two-dimensional stable invariant manifold $\mathcal{M}$, where all trajectories starting in $\mathcal{M}$ converge to the undesired equilibrium point (Guckenheimer and Holmes, 1983). Since the zero eigenvalue has no influence on the solution, all trajectories converging to the undesired equilibrium lie in $\mathcal{M}$. We conclude that all trajectories except those starting in $\mathcal{M}$ converge to the desired equilibrium. Since the dimension of $\mathcal{M}$ is two, it has measure zero in the state space $T\mathbb{S}^2$, and we say that the domain of attraction of the desired equilibrium point is almost global.

REFERENCES

Beard, R.W. and McLain, T.W. (2012). *Small Unmanned Aircraft*. Princeton University Press, Princeton, NJ.

Bhat, S.P. and Bernstein, D.S. (2000). A topological obstruction to continuous global stabilization of rotational motion and the unwinding phenomenon. *Syst. Control Lett.*, 39(1), 63–70.

Bullo, F., Murray, R., and Sarti, A. (1995). Control on the sphere and reduced attitude stabilization. *IFAC Proc. Vol.*, 28(14), 495–501.

Casau, P., Mayhew, C.G., Sanfelice, R.G., and Silvestre, C. (2019). Robust global exponential stabilization on the n-dimensional sphere with applications to trajectory tracking for quadrotors. *Automatica*, 110, 108534.

Chaturvedi, N. and McClamroch, H. (2009). Asymptotic stabilization of the inverted equilibrium manifold of the 3-D pendulum using non-smooth feedback. *IEEE Trans. Autom. Control*, 54(11), 2658–2662.

Chaturvedi, N., Sanyal, A., and McClamroch, H. (2011). Rigid-body attitude control. *IEEE Control Syst.*, 31(3), 30–51.

Chaturvedi, N., McClamroch, N., and Bernstein, D. (2009). Asymptotic smooth stabilization of the inverted 3-D pendulum. *IEEE Trans. Autom. Control*, 54(6), 1204–1215.

Guckenheimer, J. and Holmes, P. (1983). *Nonlinear Oscillations, Dynamical Systems, and Bifurcations of Vector Fields*. Springer-Verlag, New York, NY.

Johansen, T.A., Zolich, A., Hansen, T., and Sorensen, A.J. (2014). Unmanned aerial vehicle as communication relay for autonomous underwater vehicle — Field tests. In *2014 IEEE Globecom Workshops (GC Wkshps)*, 1469–1474.

Khalil, H.K. (2002). *Nonlinear Systems*. Prentice-Hall, Upper Saddle River, NJ, USA.

Lee, T. (2015). Global exponential attitude tracking controls on SO(3). *IEEE Trans. Autom. Control*, 60(10), 2837–2842.

Lee, T. (2016). Optimal hybrid controls for global exponential tracking on the two-sphere. In *2016 IEEE 55th Conference on Decision and Control (CDC)*, 3331–3337.

Lee, T., Leok, M., and McClamroch, N.H. (2011). Stable manifolds of saddle equilibria for pendulum dynamics on S2 and SO(3). In *2011 50th IEEE Conference on Decision and Control and European Control Conference*, 3915–3921.

Markley, F.L. and Crassidis, J.L. (2014). *Fundamentals of Spacecraft Attitude Determination and Control*. Springer-Verlag, New York, NY.

Mayhew, C.G. and Teel, A.R. (2013). Global stabilization of spherical orientation by synergistic hybrid feedback with application to reduced-attitude tracking for rigid bodies. *Automatica*, 49(7), 1945–1957.

Meier, L., Honegger, D., and Pollefeys, M. (2015). PX4: A node-based multithreaded open source robotics framework for deeply embedded platforms. In *2015 IEEE International Conference on Robotics and Automation (ICRA)*, 6235–6240.

Ramp, M. and Papadopoulos, E. (2015). Attitude and angular velocity tracking for a rigid body using geometric methods on the two-sphere. In *2015 European Control Conference (ECC)*, 3238–3243.

Reinhardt, D., Coates, E.M., and Johansen, T.A. (2020). Hybrid control of fixed-wing UAVs for large-angle attitude maneuvers on the two-sphere. In *2020 21st IFAC World Congress*.

Stevens, B.L., Lewis, F.L., and Johnson, E.N. (2016). *Aircraft Control and Simulation*. Wiley-Blackwell, Hoboken, NJ.

Wen, J.Y. and Kreutz-Delgado, K. (1991). The attitude control problem. *IEEE Trans. Autom. Control*, 36(10), 1148–1162.

Wrzos-Kaminska, M., Pettersen, K., and Gravdahl, J. (2019). Path following control for articulated intervention-AUVs using geometric control of reduced attitude. *IFAC-PapersOnLine*, 52(16), 192–197.